POLISH MARITIME RESEARCH 3 (123) 2024 Vol. 31; pp. 102-112
10.2478/pomr-2024-0040

Study of Predictive Control Model for Cooling Process of Mark III LNG Bunker

Guozhi Bao *1
Weiguang Qin 2
Qingfeng Jiang 2
Chunrong Pu 3
1 School of Energy and Power, Jiangsu University of Science and Technology, Zhenjiang, Jiangsu, China
2 Department of Energy and Power, Jiangsu University of Science and Technology, Zhenjiang Jiangsu, China
3 China Resources (Nanjing) Municipal Design Co., Ltd., Nanjing, Jiangsu, China

* Corresponding author: *gzbao2005@163.com (Guozhi Bao)*

ABSTRACT

When loading liquefied natural gas (LNG) onto a dual-fuel LNG container ship fuelled by LNG, there is a considerable temperature difference between LNG and the fuel tank at room temperature. The current solution is to pre-cool the tank with LNG through a spray line but the cooling process, if not correctly handled, can result in excessive cooling rates and Boil-Off Gas (BOG), which can expose the tank to increased temperature stress and gas pressure. Therefore, this paper takes the Mark III fuel tank of a specific type of LNG container ship as the object and realises a real-time predictive control system by writing a UDF (User Defined Function) to simulate and analyse the influence of LNG spray rate on the change of cooling effect, cooling time and cooling cost under the unidirectional LNG spray cooling mode. Compared with the results of the fuel tank gas experiment, the deviation of numerical model simulation results is less than 5%. Under the same cooling rate, the real-time control scheme can achieve a more uniform cooling rate and reduce the total LNG consumption by 25%. With the increase in LNG cooling rate, the cooling time, LNG usage, and the total BOG exhaust volume all decrease; however, the decreased range gradually decreases as well. The results of this paper provide parameters and suggestions for optimising and improving the LNG fuel tank cooling monitoring and control system.

Keywords: LNG tank cooling process; prediction and control; CFD simulation; thermal performance; cost analysis

INTRODUCTION

In recent years, since the International Maritime Organization (IMO) proposed the global maritime sulphur content limit in 2020 [1], the environmental regulations related to sulphur oxides and nitrogen oxides have been tightened in various regions [2]. LNG has attracted more attention from all walks of life because it is relatively clean, has high-energy efficiency [3] and abundant reserves sufficient to meet global natural gas demand [4]. However, due to the ultra-low temperature characteristics of liquefied natural gas, it is generally transported and stored at 111.15 K under normal pressure [5]. LNG, whether as a cargo or fuel, must be thoroughly cooled before entering the LNG Cargo Containment System (CCS) [6]. The cooling rate is generally controlled at 10 K/hr [7] in order to avoid the thermal stress caused by extreme temperature changes and the damage to the bulkhead caused by the rapid increase of pressure in the tank [8]. The CCS cooling medium is mainly liquid nitrogen or LNG. Compared with liquid nitrogen cooling, LNG cooling has the advantages of a short cooling time and small liquid consumption and is more suiTable for large storage equipment. However, because the market price of LNG is higher than that of liquid nitrogen, the overall cooling cost of LNG is higher than that of liquid nitrogen [9]. In order to improve the utilisation efficiency of LNG in the cooling process in a fuel tank, one method is to re-liquidise [10] and recycle the BOG produced by it [11] or reuse its excess cold energy [12]; the other method is to closely control the supply rate of LNG. Therefore, it is necessary to establish a predictive control model for the process of cooling the tank by atomisation and evaporation of the spray cooling medium, which can accurately predict the dynamic cooling of the tank, provide feedback on the results, and control the liquid inlet velocity of the cooling medium to provide a reliable reference for onshore LNG filling operations.

Research into the dynamic low temperature characteristics of CCS has been pursued for some time. For example, Lu et al. (2016) [13] used computational fluid dynamics (CFD) models to study the temperature gradient between the storage tank membrane and the insulating layer during the cooling operation of the storage tank membrane on LNG carriers. Xia et al. (2023) [14] constructed a numerical model of the liquid nitrogen cooling process for a large horizontal storage tank, to study the maximum deformation position of the tank and the distribution law of thermal stress under the fixed liquid nitrogen inlet flow rate. However, the input and output of the tank were dynamically adjusted according to the operating state of the tank. Based on the specifications and guidelines for CCS acceptance and LNG filling operations issued by the national classification societies and the International Maritime Organization, most work can usually be carried out within a controllable and safe range. For example, the China Classification Society has a 10 m/s limit for the maximum filling rate of liquefied natural gas fuel [15]. Niu et al. (2020) [16] studied the liquid nitrogen Boil-Off Rate (BOR) of the independent B-type tank under the International Gas Code (IGC) conditions. Jo et al. (2021) [17] carried out mathematical modelling of unsteady LNG storage tanks in a ventilated state and sealed tank mode, accurately estimating the changes in pressure and temperature during the operation of LNG storage tanks and formulated corresponding operation strategies according to different initial filling ratios. Wang et al. (2021) [18] analysed the condensation and cooling effect of steam during the top spray filling process, resulting in the sealed tank mode; the filling temperature and droplet diameter significantly affected the filling effect. Jo et al. (2021) [19] proposed an offset-free model predictive control (MPC) system to adjust the storage pressure of LNG storage tanks and proved that the offset-free MPC system can still adjust the pressure in the case of a fire accident. Similarly, Shin et al. (2022) [20] studied the dynamic process of controlling inlet spray and outlet BOG flow in an MPC designed for LNG tank cooling. Wu et al. (2023) [21] established the digital twin (DT) model of a steady-state temperature field, which realised the research and monitoring of the temperature field of the entire LNG storage tank.

In the current numerical studies of tank cooling processes, the inlet rate of the cooling medium is constant. The input and output control of the complete filling system, from the LNG filling station to the storage tank on board, still needs manual operation. In this paper, based on the experimental process of tank cooling of a dual fuel ship, the finite element analysis model of the cooling process is established by using Ansys Fluent series software. MPC is implemented by providing UDFs (User-Defined Functions) in the Fluent solver for program editing [22]. Firstly, four different monitoring periods are simulated and the appropriate and safe monitoring period obtained. Secondly, five different fuel tank cooling rate control schemes are simulated under the selected monitoring period and the effects of different cooling rate schemes on cooling stability, cooling time, and cooling cost are discussed. The results provide a useful reference and suggestions are made for the monitoring and control of a LNG tank cooling process.

NUMERICAL METHODS AND MODELS

As shown in Fig. 1, the CCS in this paper is a MARK III LNG fuel tank of a dual-fuel power container ship. The detailed geometric parameters are summarised in Table 1. The total volume of the tank was 18,600 m^3. The bulkhead mainly comprised 1.2 mm 304L alloy steel, 12 mm laminate, a 100 mm polyurethane foam secondary insulation layer, a 170 mm polyurethane foam primary insulation layer, and 9 mm of laminate from the inside to the outside. The gas outlet pipe had a diameter of 0.2 m and the liquid inlet pipe contained 25 nozzles with a diameter of 0.0075 m, located on the same side of the tank. The schematic diagram of the cooling experiment is shown in Fig. 2. The tank was filled with natural gas at 297.15 K in the initial condition. The air temperature outside the tank was 303.15 K. The initial pressure in the tank was 141 kPa and the BOG emission mode of LNG during the cooling process adopted a differential pressure emission.

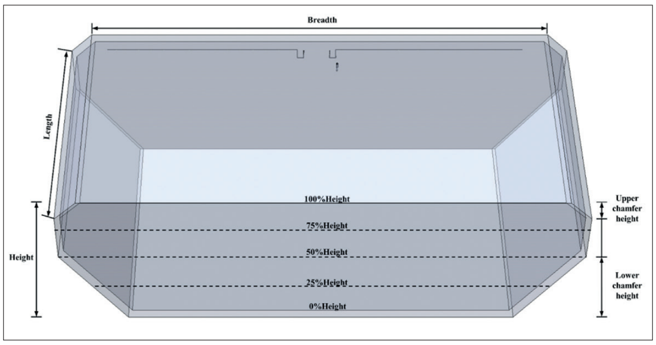

Fig.1. Schema of MARK III LNG fuel tank

Tab. 1. Geometry of LNG tank

Parameter	Unit	Value
Tank breadth	m	52.245
Tank length	m	24.025
Tank height	m	17.565
Tank upper chamfer height	m	3.0145
Tank lower chamfer height	m	8.7945

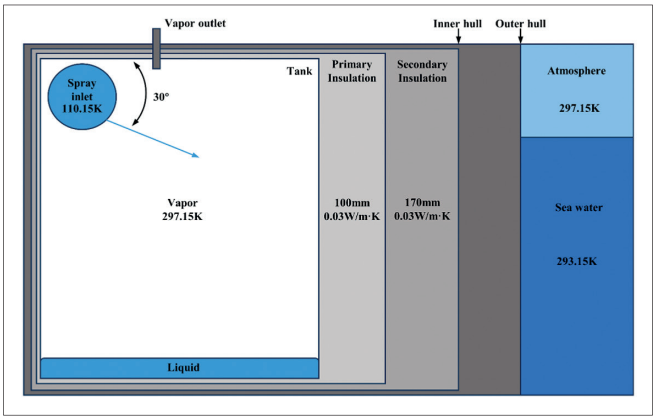

Fig.2. Schematic diagram of LNG spray and environmental heat transfer in fuel tank

In this paper, the numerical modelling and solution of the cooling process of the fuel tank are studied by using Ansys Fluent software. In the numerical simulation in Ansys Fluent, the discrete phase model (DPM) describes the discrete phase motion of the coolant droplet and its interaction with the continuous phase [23]. The Navier-Stokes equations solve the continuous phase's mass, momentum and energy transfer [24]. The KH-RT crushing model was selected as the secondary crushing model [25] for the pressure swirl nozzles. The SST k-ω turbulence model with enhanced wall treatment was selected to achieve the pressure-velocity coupling method of the SIMPLEC algorithm.

The equations of the continuous phase are shown below:

Mass conservation equation:

$$\frac{\partial\rho}{\partial t} + \frac{\partial}{\partial x}(\rho u_k) + \frac{\partial}{\partial y}(\rho u_S) + \frac{\partial}{\partial z}(\rho u_L) = S_m \quad (1)$$

Momentum conservation equation:

$$\frac{\partial}{\partial t}(\rho u_x) + \nabla\cdot(\rho u_x U) = -\frac{\partial\rho}{\partial x} + \nabla\cdot(\mu\nabla u_x) + F_x \quad (2)$$

$$\frac{\partial}{\partial t}(\rho u_y) + \nabla\cdot(\rho u_y U) = -\frac{\partial\rho}{\partial y} + \nabla\cdot(\mu\nabla u_y) + F_y \quad (3)$$

$$\frac{\partial}{\partial t}(\rho u_z) + \nabla\cdot(\rho u_z U) = -\frac{\partial\rho}{\partial z} + \nabla\cdot(\mu\nabla u_z) + F_z \quad (5)$$

Energy conservation equation:

$$\frac{\partial}{\partial t}(\rho E) + \nabla\cdot[U(\rho E + p)] = \nabla\cdot\left[k_e\nabla T - \sum_j J_j\int_{T_{ref}}^{T} c_{p,j}dT + (T_e\cdot U)\right] + Q \quad (5)$$

The equations of the discrete phase are:

Mass, momentum, and energy transfer equations for droplet trajectory:

$$m_p\frac{du_{p,x}}{dt} = m_p\frac{u_x - u_{p,x}}{\tau_r} + m_p\frac{g_x(\rho_p - \rho)}{\rho_p} \quad (6)$$

$$m_p\frac{du_{p,y}}{dt} = m_p\frac{u_y - u_{p,y}}{\tau_r} + m_p\frac{g_y(\rho_p - \rho)}{\rho_p} \quad (7)$$

$$m_p\frac{du_{p,z}}{dt} = m_p\frac{u_y - u_{p,z}}{\tau_r} + m_p\frac{g_z(\rho_p - \rho)}{\rho_p} \quad (8)$$

The particle relaxation time τ_r was calculated according to the relative Reynolds number $Re = \rho d_p|\vec{u}_p - \vec{u}\,|/\mu$.

$$\tau_r = \frac{24\rho_p d_p^2}{18\mu C_D Re} \quad (9)$$

The particle trajectory equations are:

$$\frac{dx}{dt} = u_{p,x} \quad (10)$$

$$\frac{dy}{dt} = u_{p,y} \quad (11)$$

$$\frac{dz}{dt} = u_{p,z} \quad (12)$$

The droplet size was predicted by the Rosin-Rambler distribution: $Y_d = e^{-(d_p/\bar{d})^n}$.

The droplet temperature was calculated by Eq. (13), in which the convective heat transfer and radiative heat transfer are considered:

$$T_p(t + \Delta t) = \alpha_p + [T_p(t) - \alpha_p]e^{-\beta_p\Delta t} \quad (13)$$

where $\alpha_p = (h'T'_\infty + \varepsilon_p\sigma'\theta_R^4)/[h' + \varepsilon_p\sigma'T_p^3(t)]$ and $\beta_P = [A_P(h' + \varepsilon_p\sigma'T_P^3(t))]/(m_p c_P)$.

The heat transfer coefficient h' was calculated by (14).

$$h' = \frac{k}{d_p(2 + 0.6Re^{0.5}Pr^{\frac{1}{3}})} \quad (14)$$

The two-way coupling equations [26] between the unit droplet and the continuous phase are as follows:

$$Q = \left(\frac{\overline{m_p}}{m_{p,0}}c_p\Delta T_p + \frac{\Delta m_p}{m_{p,0}}\left(-h_{fg} + \int_{T_{ref}}^{T_p} c_p dT\right)\right)m'_{p,0} \quad (15)$$

$$F_x = \Sigma\left(\frac{3\mu C_D Re}{4\rho_p d_p^2}(u_{p,x} - u_x)\right)m'_p\Delta t \quad (16)$$

$$F_y = \Sigma\left(\frac{3\mu C_D Re}{4\rho_p d_p^2}(u_{p,y} - u_y)\right)m'_p\Delta t \quad (17)$$

$$F_z = \Sigma\left(\frac{3\mu C_D Re}{4\rho_p d_p^2}(u_{p,z} - u_z)\right)m'_p\Delta t \quad (18)$$

$$S_m = \frac{Am_p}{m'_{p,0}}m'_{p,0} \quad (19)$$

where $\overline{m_p}$ is the average mass of the droplet in the control volume, $m_{p,0}$ is the initial mass of the droplet, Δm_p is the mass change of the droplet through each control volume, m'_p is the initial mass flux of the droplet, and ΔT_p is the temperature change of the droplet in the control volume.

The transport equations for the SST k-ω model is given by Eqs. (20) and (21).

$$\rho\frac{\partial(ku_i)}{\partial x_i} = \frac{\partial}{\partial x_j}\left(\Gamma_k\frac{\partial K}{\partial x_j}\right) + G_K - Y_k \quad (20)$$

$$\rho\frac{\partial(\omega u_i)}{\partial x_i} = \frac{\partial}{\partial x_j}\left(\Gamma_\omega\frac{\partial\omega}{\partial x_j}\right) + G_\omega - Y_\omega + D_\omega \quad (21)$$

$$\Gamma_k = (\mu + \sigma_K\mu_t);\ G_K = \tau_{ij}\frac{\partial u_i}{\partial x_j};\ Y_k = \beta^*\rho\omega K \quad (22)$$

$$\Gamma_\omega = (\mu + \sigma_\omega\mu_t);\ G_\omega = \frac{\gamma}{\nu_t}\tau_{ij}\frac{\partial u_i}{\partial x_j};\ Y_\omega = \beta\rho\omega^2;$$

$$D_\omega = 2(1 - F_1)\rho\sigma_{\omega 2}\frac{1}{\omega}\frac{\partial k}{\partial x_j}\frac{\partial\omega}{\partial x_j} \quad (23)$$

where k is the turbulent kinetic energy, ω is the specific dissipation rate, Γ_k and Γ_ω are the effective diffusivity of k and ω, G_K and G_ω represent the generation of k and ω, respectively, Y_k and Y_ω represent the dissipation of k and ω due to turbulence, and D_ω is the cross-diffusion term.

In numerical simulations, the wall of the tank was simplified and set as a non-slip boundary. Its equivalent heat transfer coefficient was 0.108 w/m·K. The outlet was set to the pressure outlet condition and the tank was initially loaded with 297.15 K natural gas at a pressure of 141 kPa. The remaining boundary was set to a pressure of 101.325 kPa. A two-phase flow simulation was involved and the physical parameters of LNG's two phases are shown in Table 2.

Tab. 2. Thermophysical parameters of LNG and its evaporated gas

Parameter	Unit	LNG	Vapour
Density (ρ)	kg/m^3	443.5	1.6
Specific heat capacity (C_p)	$kJ/kg{\cdot}K$	3408	2222
Thermal conductivity (k)	$w/m{\cdot}K$	0.332	0.209
Dynamic viscosity (μ)	$kg/m{\cdot}s$	1.176E-4	1.087E-5
Latent heat of vapourisation (r)	kJ/kg	522.5	/

MODEL VERIFICATION

The numerical model was based on the full dimension of the fuel tank, ignoring the influence of other lines in the bunker dome and the loss of (water) head between the LNG inlet pipe and the nozzle. It was assumed that the LNG inlet pipeline uniformly supplies LNG to 25 nozzles. The grid model encrypts areas above the height of the spray pipe and areas near to no walls. In this paper, by comparing the numerical model with the gas test data of the fuel tank of a dual-fuel ship before leaving the factory, the grid independence verification and accuracy verification of the model were completed. Due to the single-side spray scheme of the fuel tank, the vertical wall near to the spray line was cooled most fully, being the best reflection of the cooling uniformity in the direction of height; this parameter is also an important index for testing the safe operation of the fuel tank. Therefore, the independence verification of the grid model was first completed by comparing the average temperature of the numerical model and the experimental data on the wall surface. Secondly, the average temperature of five different heights were taken on the wall surface, to test the accuracy of the model. These included 0% Height (the bottom of the wall), 25% Height, 50% Height, 75% Height, and 100% Height (the top of the wall).

In order to verify the grid independence of the numerical model, four sets of grid models were established in this paper, as shown in Fig. 3, with the number of grids being 1.28 million, 1.83 million, 3.82 million and 5.12 million, respectively.

The spray inlet flow rate during the cooling experiment is shown in Fig. 4. The initial experimental spray flow rate Q_p of 0.465 tons/hr gradually decreases to the lowest value Q_{p1}. Obviously, the ideal initial LNG spray flow rate Q_{p0} is smaller. However, due to some working characteristics of LNG supply systems, the initial spray flow rate is often difficult to accurately match Q_{p0} and often starts with a larger value.

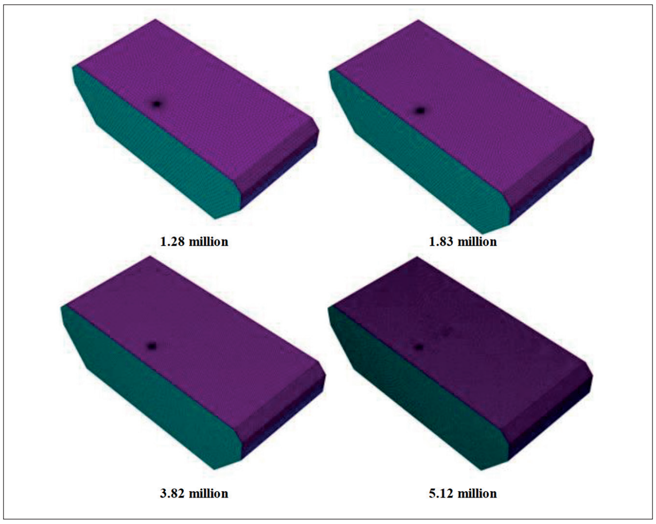

Fig. 3 Schematic diagram of grid division

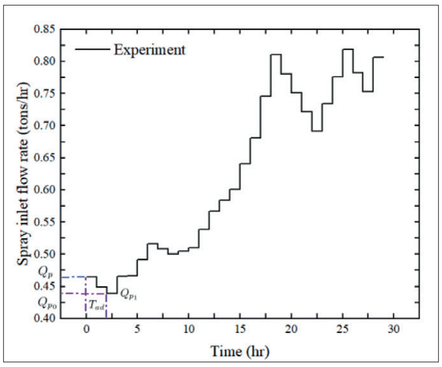

Fig.4. Spray inlet flow rate of the experiment

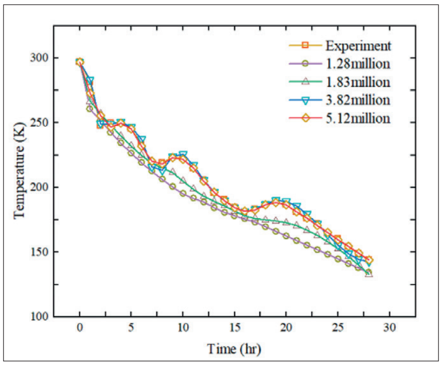

Fig.5. The average temperature of the fuel tank varies with thenumber of grids

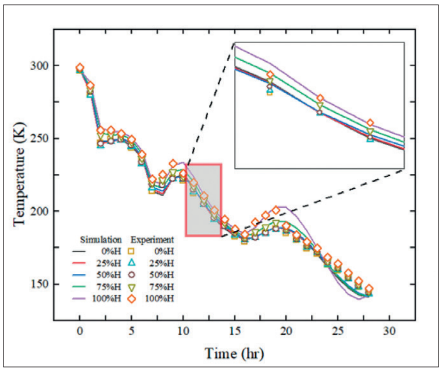

Fig.6. Wall temperatures by numerical model for verification

The average temperature of the wall surface varies with the number of grids, as shown in Fig. 5. By comparing different curves, it can be seen that, although the general trend of all curves decreases according to the power law, and with the change of inlet flow rate, there will be wavy fluctuations when the temperature rises. It is obvious that, with the increase in the number of grids, the change curve of average temperature is more consistent with the curve measured in the experiment. Fig. 6 shows the variation of average temperature of the 3.82 million grid model at different heights of the wall. When the number of grids reaches 3.82 million, the relative error of the calculated results can not only be controlled within 5%, but the spatial distribution of the average temperature also has a high agreement with the experimental results; increasing the number of grid units has little influence on the numerical results. Considering the calculation accuracy and efficiency, the numerical model of the 3.82 million grid was selected to study the thermodynamic law of the cooling process of the fuel tank. The numerical model has an average quality of 0.9766, an average skewness of 0.418, and includes five boundary layers with a y^+ value of 5 [27].

MPC DESIGN OF COOLING PROCESS

According to the research and analysis of the relevant cooling LNG storage tank [28], the instability of the spray pressure control of the cooling medium is the main reason for the uneven temperature drop of the storage tank; the spray pressure has little effect on the pressure in the tank. Therefore, the exhaust mode of the fuel tank studied in this paper is the differential pressure exhaust mode, i.e. the exhaust valve remains fully open. The spray pressure determines the flow rate of the cooling medium entering the fuel tank. The input rate of the cooling medium is the main factor affecting the cooling effect, cooling safety and cooling cost [29]. The control of the inlet flow rate depends on the temperature difference between the upper and lower parts of the fuel tank during the cooling process, the temperature drop rate, and the pressure rise rate in the tank. By adjusting the opening of the valves, such as the liquid phase valve and the vapouriser in the tank, the fuel tank is uniformly cooled and the pressure in the tank does not exceed the design range. The following coolant filling principles can be obtained from the comprehensive fuel tank filling safety manual and the relevant inspection specifications and guidelines for liquid natural gas ships, published by the China Classification Society.

(1) Pressure control: the maximum allowable working pressure of the fuel tank is 0.07 MPa and the pressure control range of the cooling tank is 0.004-0.061 MPa. The primary insulated space (IBS) pressure control is 0.0005-0.001 Mpa and the secondary insulated space (IS) pressure control is IBS + 2 < IS < IBS + 7.
(2) Temperature control: the cooling rate of the fuel tank is generally controlled within 10 K/hr and the cooling design requirement is 143.15 K. The temperature difference between the upper wall and lower wall is not more than 50 K. When the temperature exceeds 50 K, the cooling input is immediately stopped and the cooling is performed when the temperature difference drops below 50 K. When using liquid nitrogen cooling, the bottom wall temperature is required to be not less than 110.15 K, to avoid the accumulation of liquid nitrogen and LNG.

MPC is used to dynamically control the cooling capacity input during the cooling process of the fuel tank. The main idea is to dynamically control the cooling capacity input by periodically monitoring the temperature and pressure parameters of the fuel tank. Based on this, the specific method is as follows.

(1) Adjusting the cooling input rate to ensure that the tank pressure of the fuel tank is within the control range of 0.004-0.061 MPa. If it is lower or higher than the pressure control range, the cooling input rate is preferentially adjusted to ensure that the tank pressure is reasonable. However, based on the above analysis, the tank pressure under a differential pressure exhaust is, basically, within a reasonable range and the control is a pressure insurance mechanism.
(2) After ensuring that the tank pressure is reasonable, the cooling input rate is adjusted to ensure uniform cooling of the fuel tank. If the maximum temperature difference of all bulkheads exceeds 50 K, the cooling input is adjusted to 0. When the temperature difference is below 50 K, the cooling input starts from 0. The control is a temperature difference insurance mechanism.
(3) After the pressure and temperature distribution of the fuel tank are within a reasonable range, the cooling rate of the fuel tank is subdivided by adjusting the cooling input. The cooling rate control of the fuel tank can be divided into two categories: the overall cooling rate and the periodic cooling rate. The overall cooling rate refers to the cooling rate from the beginning of cooling to the current time. The cooling rate of the cycle refers to the cooling rate from the beginning to the end of the current cycle. Firstly, if the overall cooling rate is within the preset cooling rate interval, the cooling input is adjusted according to the periodic cooling rate. If the periodic cooling rate is higher than the preset interval, the cooling input is reduced and, if it is less than the preset interval, the cooling input is increased. Secondly, if the overall cooling rate is greater than the preset interval, the cooling input is directly reduced. If it is less than the preset interval then cooling input is increased and the periodic cooling rate is no longer judged.

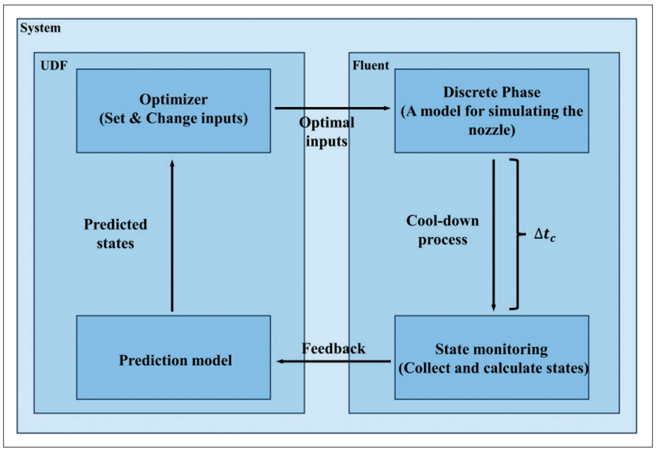

Fig.7. Schematic diagram of MPC operation

Tab. 3. Specific control parameters of MPC

Rule	Description	Unit	Values
1	The temperature at the end of the cooling process, T_w	K	T_t=T_w=143.15
2	Tank pressure control range, P_E	Mpa	[0.004, 0.061]
3	Maximum temperature difference, $\|\Delta T_{max}\|$	K	[0,50]
4	The overall cooling rate = The periodic cooling rate, $\|dT\|$	K/hr	[0,10]
5	The maximum allowable cooling rate deviation, $\|\Delta T_E\|$	K	[0,0.5]
6	Monitoring period, Δt_c	hr	[1/20,1/3]
7	Adjustment value of spray inlet flow rate in Δt_c, $\|\Delta Q\|$	Tons/hr	0.072

Fig. 7 shows that the basic operation process of MPC is that the initial spray inlet flow rate Q_p set by each nozzle is the initial value of the experiment at the beginning of the spray. After the spray cooling of each monitoring period, the average temperature T_0, $T_{0.25}$, $T_{0.5}$, $T_{0.75}$, or T_1 of all unit nodes on five different wall heights, the maximum temperature difference ΔT_{max} between any two nodes (in general between the top surface and the bottom surface), the average temperature T_t of all walls, and the average pressure of the fuel tank are calculated and fed back to the MPC (written by UDF). The MPC is responsible for predicting the fuel tank's cooling effect and optimising the injector's inlet velocity according to the fed back parameters. In the whole cooling process, the numerical model will undergo many monitoring periods of predictive control, to achieve the effect of model training until the average temperature of the fuel tank reaches 143.15 K[30]. The specific control parameters involved in MPC are shown in Table 3.

RESULTS AND DISCUSSION

MONITORING PERIOD

It can be seen from the experimental data in Fig. 4 and Fig. 6 that the whole tank cooling process, with an average cooling rate of 5.5 K/hr, is divided into two stages: the rapid cooling stage and the slow cooling stage. If the spray inlet flow rate is used as the basis for division, the stage before the spray inlet flow rate is reduced to Q_{p1} is the rapid cooling stage and, thereafter, it is the slow cooling stage. The rapid cooling stage lasts about 3 hrs. The general temperature feedback of the fuel tank struggles to catch up with the adjustment of the LNG spray inlet rate, especially in the rapid cooling stage. Such hysteresis brings considerable difficulty to the cooling rate control of the fuel tank and easily causes safety hazards. Therefore, in this paper, four monitoring cycles of 1/20 hr, 1/6 hr, 1/4 hr, and 1/3 hr were selected. The maximum allowable cooling rate deviation $|\Delta T_E|$ is 0.5 K. With these parameters as the reference standard for MPC operation, it is expected that the numerical model can achieve the same average cooling rate (5.5 K/hr) as the experiments.

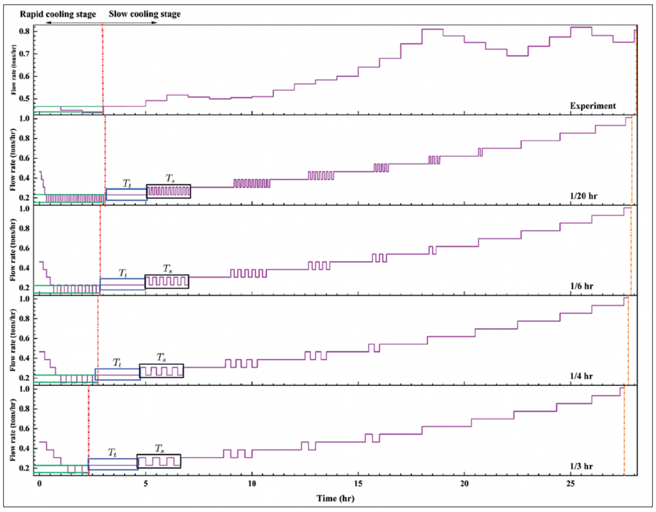

Fig. 8. Spray inlet flow rate of different monitoring periods

The changes in spray inlet velocity and other parameters, under different monitoring cycles, are shown in Fig. 8. It can be seen that the spray inlet rate is divided into a transition stage T_t and a stationary stage T_S in the slow cooling stage. The duration of the stationary stage T_S of different monitoring periods is the same, while the duration of the transition stage T_t decreases with the increase in the monitoring period and gradually disappears with the cooling process.

In Fig. 9, the temperature change is very sensitive in the rapid cooling stage. Although the MPC runs in different monitoring periods, the spray inlet flow rate of each numerical model is successfully reduced to 0.15-0.23 tons/hr within 1 hr (the interval where Q_{p1} is located). However, from the perspective of temperature performance, the temperature difference of MPC in different monitoring periods is still obvious in the rapid cooling stage. The cooling rate is also difficult to control. A monitoring

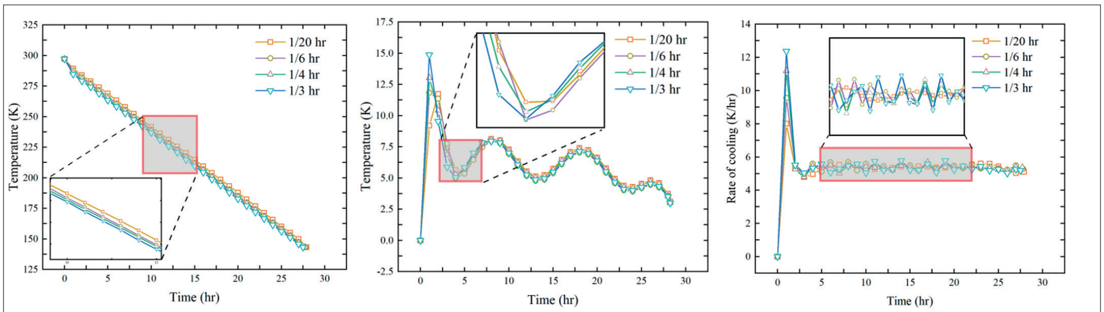

(a) The average temperature of the fuel tank (b) Maximum temperature difference of the fuel tank (c) The actual cooling rate of the fuel tank

Fig. 9. The parameter variation with the expected cooling rate of 5.5 K/hr under different monitoring periods

period of 1/3 hr is enough to cause the fuel tank cooling rate to exceed the 10 K/hr limit. Therefore, the influence of the monitoring period on the rapid cooling stage cannot be ignored. The contribution of the monitoring cycle to cooling safety is much more significant than the cooling effect. In other words, reducing the cost of LNG in the cooling process is not accessible by increasing the monitoring frequency ($1/\Delta t_c$). The parameters under the monitoring period of 1/20 hr are reasonable with the limit requirements and have the operability of engineering applications. Therefore, the monitoring period selected by the subsequent research on the cooling rate of the fuel tank is 1/20 hr.

RATE OF COOLING

The maximum allowable cooling rate deviation of MPC is still 0.5 K/hr and the monitoring period is set at 1/20 hr. In order to analyse the influence of different cooling rates, five different expected cooling rates (4 K/hr, 5.5 K/hr, 7 K/hr, 8.5 K/hr, and 10 K/hr) were designed. According to the above analysis of the initial spray inlet flow rate, the cooling process of each case, under different expected cooling rates, will also be divided into the rapid cooling stage and the slow cooling stage.

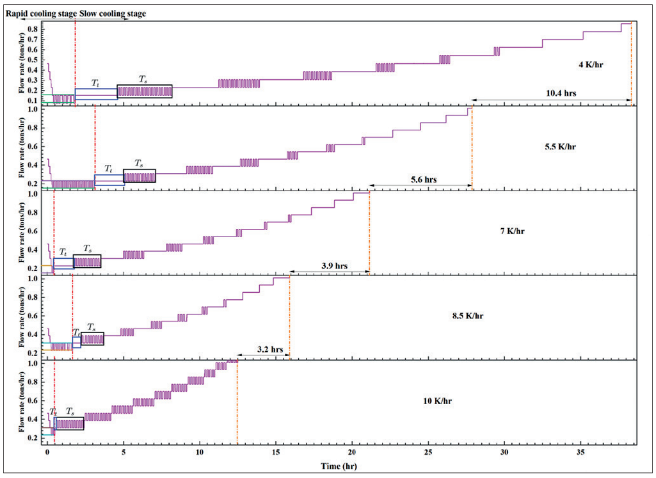

Fig.10. Spray inlet flow rates at different expected cooling rates

Fig. 10 shows that the inlet flow rate of LNG spray is increased nonlinearly with time, in order to achieve the expected cooling rate. The expected cooling rates are numerically independent under the maximum cooling rate deviation of 0.5 K/hr. The simulation cases of different independent cooling rates are also independent of each other in the interval of Q_{p1} reached in the rapid cooling stage. In other words, the initial spray flow rates Q_p of different cooling rate schemes controlled by MPC have their own suiTable flow rate ranges (the interval of Q_{p0}). In the slow cooling stage, the distribution of the stationary stage T_S and the transition stage T_t is completely different from the distribution under the same monitoring period. As the cooling rate increases, the transition stage T_t gradually increases and the stationary stage T_S gradually decreases. Finally, in the case of 10 K/hr, the stationary stage T_S disappears completely. This means that the spray inlet flow rate needs to be frequently scheduled to stabilise the cooling rate. This conclusion is also reflected in the subsequent cooling rate. From the spray inlet flow rate (Fig. 10) and the average temperature of the fuel tank (Fig. 11(a)), the following conclusions can be obtained. The benefit of the reduction in cooling time caused by the increased cooling rate does not show the same growth benefits. Under the condition that the expected cooling rate difference is 1.5 K/hr, the benefit of cooling time caused by gradually increasing the cooling rate from 1.5 K/hr, decreases from 10.4 hours to 3.2 hours.

According to the gas flow characteristics, hot natural gas accumulates on the top surface and cold natural gas sinks, or even accumulates, over time. The maximum temperature difference between the walls will eventually appear between the top and bottom walls. The maximum temperature difference of each expected cooling rate case is shown in Fig. 11(b). The maximum temperature difference increases synchronously with the cooling rate in the rapid cooling stage. Even with the cooling rate limit of 10 K/hr, the maximum temperature difference of 22 K is lower than that of 50 K in the inspection standard and the operation guide. The adjustment interval of 5 minutes can, indeed, control the cooling effect of the cooling rate below 10 K/hr, within a relatively safe and controllable range. The subsequent maximum temperature difference is in a slow decline process from the start of the slow cooling stage to the end. The maximum temperature difference of each expected cooling rate case is finally reduced to near to, or smaller than, the expected cooling rate. Fig. 11(c) shows the achievement of each cooling rate during MPC operation. Only the expected cooling rate of nearly 10 K/hr exceeds the cooling rate limit of 10 K/hr in the rapid cooling stage. Thus, the entire LNG fuel tank cooling process can be accurately controlled as long as a more reasonable MPC is designed.

As shown in Fig. 11(d) and Fig. 11(e), when the cooling rate remains relatively stable, the average pressure in the tank first increases and then decreases with an increase in cooling time. The gasification rate was maintained at about 1 in the early stages. The main reason for this is that the early spray pressure is low. The sprayed LNG droplets with a larger particle size directly contact the superheated area in the tank and are wholly vaporised instantaneously. The pressure difference caused by the rapid pressure increase in the tank leads to an increased gas flow rate. The BOG exhaust volume also increases rapidly.

As the subsequent cooling work continues, the pressure in the tank gradually decreases and, at this time, the inlet pressure is still increasing, increasing the spray rate. According to the research, the particle size of LNG mist decreases with the increase of spray pressure and its decreasing speed also decreases gradually. The movement range of liquefied natural gas droplets is always in the hot gas accumulation zone but the degree of superheating decreases with a decrease in the temperature of the fuel tank. The gasification rate begins to decrease and liquid begins to accumulate. The decrease in gasification rate increases significantly with the increase in spray volume. At the same time, the gas flow rate in the tank also tends to be stable, so the BOG exhaust rate increases in the later period, as shown in Fig. 11(d), but the growth rate is significantly slower.

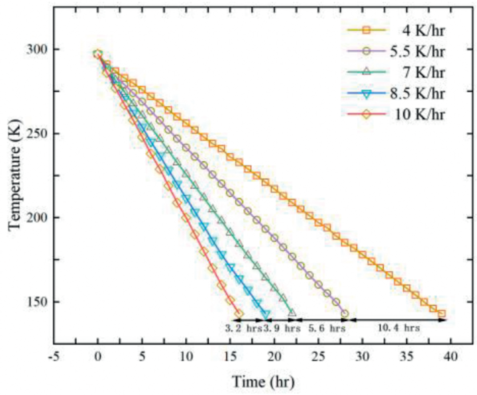

(a) The average temperature of the fuel tank

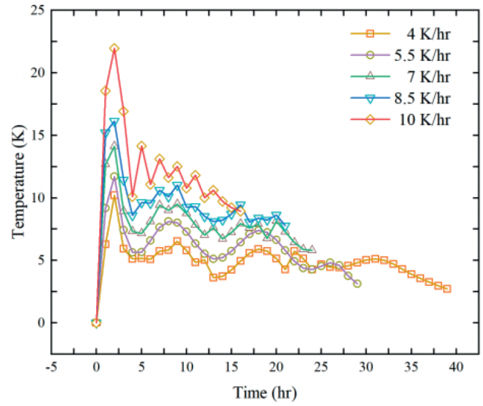

(b) Maximum temperature difference of the fuel tank

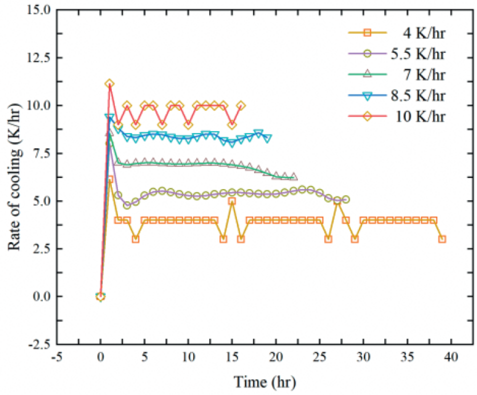

(c) The actual cooling rate of the fuel tank

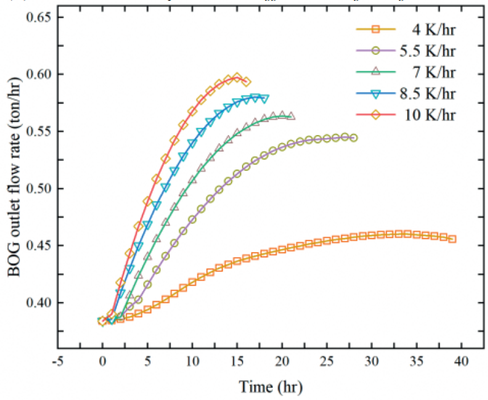

(d) BOG outlet flow rate of the fuel tank

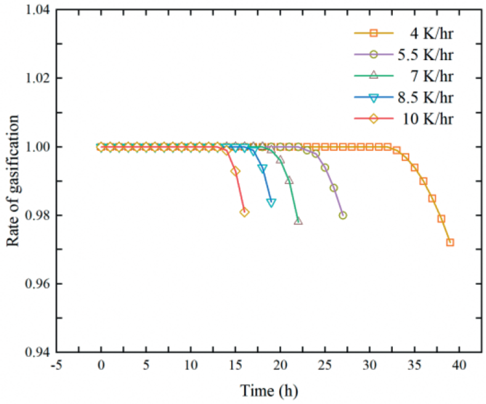

(e) The gasification rate of LNG

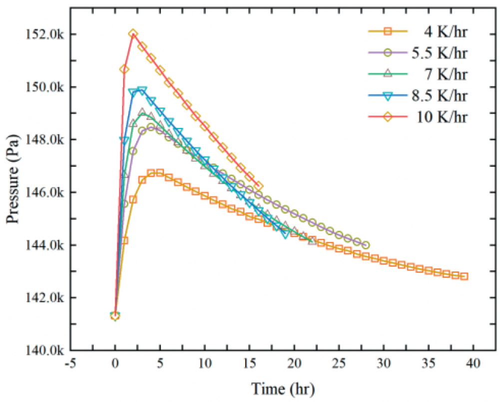

(f) The pressure of the fuel tank

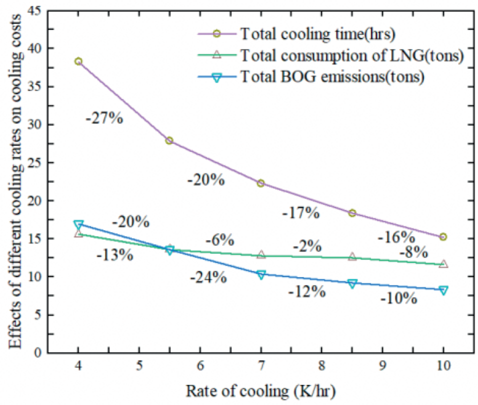

(g) Effects of different cooling rates on cooling costs

Fig. 11. The parameter distribution of the fuel tank under different expected temperature cases

As shown in Fig. 11(g), when the cooling rate increases, the LNG cooling time, total LNG consumption, and total BOG emissions show a stepwise decreasing trend at each cooling rate below the 10 K/hr limit. However, the magnitude of the reduction also decreases with the gradual increase in the cooling rate. The total amount of LNG spray during the experiment was 18.1 tons, the cooling time was 28.3 hours, and the average cooling rate was 5.5 K/hr. Compared with the expected cooling rate of 5.5 K/hr under MPC, the cooling time is almost the same, achieving a more uniform cooling effect while saving about 25% of the total LNG consumption.

CONCLUSIONS

In this paper, the cooling process of the MARK III LNG fuel tank of a dual-fuel ship is numerically simulated. By writing MPC to simulate the cooling rate adjustment strategy in the actual cooling process, the key factors are studied and these include: temperature distribution, pressure change, cooling time, cooling cost, and total emission of the fuel tank under different monitoring cycles and cooling rates. The following conclusions can be drawn.

(1) During the cooling process of large-volume CCS at a steady cooling rate, the overall growth law of LNG spray inlet flow rate is a stepwise distribution. It is basically divided into a rapid cooling stage, in which the spray inlet flow rate needs to be gradually reduced, and a slow cooling stage, in which the spray cooling rate needs to be gradually increased.
(2) The rapid cooling stage is a transition stage that requires a large regulation of the spray inlet flow rate. Different cooling rate schemes have their own suiTable spray inlet flow rate scheduling intervals in the rapid cooling stage.
(3) The slow cooling stage is divided into a transition stage and a sTable stage. With the increase in cooling rate, the transition stage occurs more frequently, while the sTable stage gradually decreases or even disappears. The existence of the sTable stage, or the duration of the sTable stage, may be one of the reference criteria for the selection of the cooling rate scheme. A longer sTable stage means less LNG supply scheduling pressure.
(4) Increasing the monitoring frequency during the cooling process can significantly improve the control of the cooling rate's stability and reduce the probability of a considerable temperature difference between the walls during the rapid cooling stage. However, increasing monitoring frequency has little effect on LNG cost and cooling time.
(5) The cooling time, LNG usage, and BOG exhaust volume all decrease with the increase in LNG cooling rate. Although the magnitude of the decrease gradually decreases with the increase in the cooling rate, to plan the LNG cooling process reasonably is of great significance, by constructing MPC to reduce the LNG cooling cost. For the example given in this paper, the total amount of LNG can be reduced by about 25% at the same cooling rate under ideal conditions.

NOMENCLATURE

c_p	Specific heat (J/kg·K))
D_ω	Cross diffusion term (kg/(m·s))
E	Energy (J/kg)
F_i	External volume force source term (N/m^3)
g	Gravitational acceleration (m/s^2)
J_j	Diffusion flux (mol/(m^2·s)
k	Turbulent kinetic energy (m^2/s^2)
k_e	Continuous phase thermal conductivity (W/(m·K)
$\overline{m_p}$	The average mass of droplets in the control volume (kg/s)
$m_{p,0}$	Initial mass of droplet (kg)
m'_p	Initial mass flux of droplet (kg/s)
Δm_p	The mass change of the droplet through each control volume (kg)
p	Pressure (Pa)
S_m	Mass source term (kg/m^3·s)
t	Time (s)
T	Temperature (K)
T'_∞	Bulk phase temperature (K)
ΔT_p	Temperature change of droplet in the control volume (K)
u_i	Velocity vector (m/s)
U	Velocity vector
Y_i	dissipation (m^2/s^2)
i, j, k	Unit vector

Greek

ε_p	Radiation coefficient
θ	Radiation temperature (K)
μ	Dynamic viscosity ($kg/m{\cdot}s$)
ρ	Density (kg/m^3)
σ'	Stephen Boltzmann constant
τ_r	Particle relaxation time (s)
ω	Specific dissipation rate (m^2/s^3)
Γ_i	effective diffusion coefficient

REFERENCES

1. HIS Markit. IMO 2020: What every shipper needs to know, Technical report, 2019.

2. Yan XW, Song H, Peng ZL, Kong HM, Cheng YP, Han LJ. Review of Research Results Concerning the Modelling of Shipping Noise, Polish Maritime Research, vol. 28, no. 2, pp. 102-115, Jun 2021. doi: 10.2478/pomr-2021-0027.

3. Song Q, Tinoco RR, Yang H, Yang Q, Jiang H, Chen Y, Chen H. A comparative study on energy efficiency of the maritime supply chains for liquefied hydrogen, ammonia, methanol and natural gas, Carbon Capture Science & Technology, vol. 4, 2022. doi: 10.1016/j.ccst.2022.100056.

4. Ediger VŞ, Berk I. Future availability of natural gas: Can it support sustainable energy transition? Resources Policy, vol. 85, 2023. doi: 10.1016/j.resourpol.2023.103824.

5. Sharanik J, Duri M, Hadjistassou C. Liquefied natural gas (LNG), in Encyclopedia of Toxicology (Fourth Edition), Wexler P, Ed. Oxford: Academic Press, 2024, pp. 871-892.

6. Jeong B, Lee BS, Zhou P, Ha S-m. Determination of safety exclusion zone for LNG bunkering at fuel-supplying point, Ocean Engineering, vol. 152, pp. 113-129, 2018/03/15/ 2018. doi: 10.1016/j.oceaneng.2018.01.066.

7. Society CC, Inspection guide for liquefied gas carrier. China Classification Society, 2018.

8. Xu G, Wang J. The dynamical thermal stress and temperature of the main member of LNG Carrier during pre-cooling process, presented at the 6th International Conference on Energy and Environmental Protection, 2017.

9. Fu H. Analysis of influencing factors of precooling process of large LNG storage tank, Contemporary Chemical Research, no. 24, pp. 70-72, 2022. doi: 10.3969/j.issn.1672-8114.2022.24.021.

10. Gómez JR, Gómez MR, Garcia RF, Catoira AD. On board LNG reliquefaction technology: a comparative study, Polish Maritime Research, vol. 21, no. 1, pp. 77-88, 2014. doi: 10.2478/pomr-2014-0011.

11. Gómez JR, Gómez MR, Garcia RF, Catoira ADM. On board LNG reliquefaction technology: a comparative study, Polish Maritime Research, vol. 21, no. 1, pp. 77-88, 2014. doi: 10.2478/pomr-2014-0011.

12. Li Y, Li B, Deng F, Yang Q, Zhang B. Research on the Application of Cold Energy of Largescale Lng-Powered Container Ships to Refrigerated Containers, Polish Maritime Research, vol. 28, no. 4, pp. 107-121, 2021. doi: 10.2478/pomr-2021-0053.

13. Lu J, Xu S, Deng J, Wu W, Wu H, Yang Z. Numerical prediction of temperature field for cargo containment system (CCS) of LNG carriers during pre-cooling operations, Journal of Natural Gas Science and Engineering, vol. 29, pp. 382-391, 2016/02/01/ 2016. doi: 10.1016/j.jngse.2016.01.009.

14. Xia M, Yuan W, Zhang Q, Zheng Y, Li P, Chen J, Xie J. Experimental and numerical analysis of the chill-down process of a large horizontal cryogenic storage tank, Applied Thermal Engineering, vol. 234, p. 121246, 2023/11/05/ 2023. doi: 10.1016/j.applthermaleng.2023.121246.

15. Society CC, Liquefied natural gas fuel filling operation guide. China Classification Society, 2021.

16. Niu WC, Lin JC, Ju YL, Fu YZ. The daily evapouration rate test and conversion method for a new independent type B LNG mock-up tank, Cryogenics, vol. 111, p. 103168, 2020/10/01/ 2020. doi: 10.1016/j.cryogenics.2020.103168.

17. Jo Y, Shin K, Hwang S. Development of dynamic simulation model of LNG tank and its operational strategy, Energy, vol. 223, 2021. doi: 10.1016/j.energy.2021.120060.

18. Wang C, Ju Y. Modelling, simulation and analysis of tank thermodynamic behaviors during no-vent LNG bunkering operations, Cryogenics, vol. 120, 2021. doi: 10.1016/j.cryogenics.2021.103373.

19. Jo Y-P, Bangi MSF, Son S-H, Kwon JS-I, Hwang S-W. Dynamic modelling and offset-free predictive control of LNG tank, Fuel, vol. 285, p. 119074, 2021/02/01/ 2021. doi: 10.1016/j.fuel.2020.119074.

20. Shin K, Son S, Moon J, Jo Y, Kwon JS-II, Hwang S. Dynamic modelling and predictive control of boil-off gas generation during LNG loading, Computers & Chemical Engineering, vol. 160, 2022. doi: 10.1016/j.compchemeng.2022.107698.

21. Wu Y, Sun J, Yang G, Cui L, Wang Z, Wang M. Research on digital twin based temperature field monitoring system for LNG storage tanks, Measurement, vol. 215, p. 112864, 2023/06/30/ 2023. doi: 10.1016/j.measurement.2023.112864.

22. An S-y, Jeong H-w, Kim O, Shim WJ. Effects of Sway and Roll Excitations on Sloshing Loads in a KC-1 Membrane LNG Tank, Polish Maritime Research, vol. 30, no. 4, pp. 43-53, 2023. doi: doi:10.2478/pomr-2023-0057.

23. Wan H, Liu PJ, He GQ, Xue ZR, Qin F, Li WQ. Experimental and numerical studies on the spray cooling of deionized water in non-boiling regime, Case Studies in Thermal Engineering, vol. 44, 2023. doi: 10.1016/j.csite.2023.102834.

24. An SY, Jeong HW, Kim O, Shim WJ. Effects of Sway and Roll Excitations on Sloshing Loads in a KC-1 Membrane LNG Tank, Polish Maritime Research, vol. 30, no. 4, pp. 43-53, Dec 2023. doi: 10.2478/pomr-2023-0057.

25. Xiao M, Bo Y. Numerical simulation of flash boiling conditions in liquid LNG spray process, Ship Engineering, vol. 39, no. 1, pp. 20-24,45, 2017. doi: 10.13788/j.cnki.cbgc.2017.01.020.

26. Wan H, He GQ, Xue ZR, Li WQ. Numerical study and experimental verification on spray cooling with nanoencapsulated phase-change material slurry (NPCMS), International Communications in Heat and Mass Transfer, vol. 123, p. 105187, 2021/04/01/ 2021. doi: 10.1016/j.icheatmasstransfer.2021.105187.

27. Ghadimi P, Tanha A, Kourabbasloo NN, Tavakoli S. Effects of Boundary Layer Control Method on Hydrodynamic Characteristics and Tip Vortex Creation of a Hydrofoil, Polish Maritime Research, vol. 24, no. 2, pp. 27-39, Jun 2017. doi: 10.1515/pomr-2017-0047.

28. Zhu M, Li KX, Lin K-C, Shi W, Yang J. How can shipowners comply with the 2020 global sulphur limit economically?

Transportation Research Part D: Transport and Environment, vol. 79, 2020. doi: 10.1016/j.trd.2020.102234.

29. Qiu C, Yang C, Zhang J, Li Y, Bao G, Pu C. The key technology of pre-cooling filling in LNG powered ship fuel tank (in chinese), Marine Seismic Streamer Technology, vol. 50, no. 2, pp. 67-72, 2022. doi: 10.12225/j.issn.1000-3878.2022.02.20220213.

30. Bangi MSF, Kwon JS-I. Deep hybrid modelling of chemical process: Application to hydraulic fracturing, Computers & Chemical Engineering, vol. 134, p. 106696, 2020/03/04/ 2020. doi: 10.1016/j.compchemeng.2019.106696.